



HAL
open science

On the Systematic Occurrence of Compound Cold Spells in North America and Wet or Windy Extremes in Europe

Gabriele Messori, Davide Faranda

► **To cite this version:**

Gabriele Messori, Davide Faranda. On the Systematic Occurrence of Compound Cold Spells in North America and Wet or Windy Extremes in Europe. *Geophysical Research Letters*, 2023, 50 (7), 10.1029/2022GL101008 . hal-03764706v2

HAL Id: hal-03764706

<https://hal.science/hal-03764706v2>

Submitted on 17 Feb 2023

HAL is a multi-disciplinary open access archive for the deposit and dissemination of scientific research documents, whether they are published or not. The documents may come from teaching and research institutions in France or abroad, or from public or private research centers.

L'archive ouverte pluridisciplinaire **HAL**, est destinée au dépôt et à la diffusion de documents scientifiques de niveau recherche, publiés ou non, émanant des établissements d'enseignement et de recherche français ou étrangers, des laboratoires publics ou privés.

1 **On the Systematic Occurrence of Compound Cold Spells in North America and Wet** 2 **or Windy Extremes in Europe**

3 **Gabriele Messori^{1,2} Davide Faranda^{3,4,5}**

4 1. Department of Earth Sciences and Centre of Natural Hazards and Disaster Science (CNDS), Uppsala University, Uppsala, Sweden.

5 2. Department of Meteorology and Bolin Centre for Climate Research, Stockholm University, Stockholm, Sweden.

6 3. Laboratoire des Sciences du Climat et de l'Environnement, LSCE/IPSL, CEA-CNRS-UVSQ, Université Paris-Saclay, Gif-sur-Yvette, France.

7 4. London Mathematical Laboratory, London, UK.

8 5. LMD/IPSL, École Normale Supérieure, PSL research University, Paris, France.

9 Corresponding author: Gabriele Messori (gabriele.messori@geo.uu.se)

10 11 Key Points:

- 12 • North American cold spells and European wet or windy extremes are very strongly coupled
13 to recurrent large-scale atmospheric patterns.
- 14 • The compound occurrence of North American cold spells and European wet or windy
15 extremes is associated with common atmospheric patterns.
- 16 • These compound extremes show weaker evidence of common atmospheric patterns than
17 all temperature, precipitation and wind anomalies.
18

19 **Abstract**

20 The repeated co-occurrence of cold spells over Eastern North America and wet or windy extremes
21 over Western Continental Europe during recent winters, has led to hypothesise a link between the
22 two. Here, we analyse the interplay between the large-scale atmospheric circulation and co-
23 occurring cold spells in North America and wet or windy extremes in Europe. We collectively
24 term these occurrences compound cold–wet–windy extremes. We leverage a recent approach
25 grounded in dynamical systems theory, which provides an analytically and computationally
26 efficient analysis of spatially resolved, multivariate climate extremes. We find that there are
27 specific, recurrent large-scale atmospheric circulation patterns systematically associated with both
28 the individual extremes and co-occurring cold–wet–windy anomalies. Evidence for this is also
29 found when focussing on compound cold–wet–windy extremes, although with a weaker signal.
30 This motivates further analyses focussing specifically on the statistics and drivers of these
31 compound extreme occurrences.

32 **Plain Language Summary**

33 In recent winters, very cold weather over the eastern part of North America and stormy weather or
34 heavy rainfall in Europe have often made the news. One may think that these events are
35 independent, since they occur several thousands of kilometres apart. However, researchers have
36 hypothesised that there may be weather patterns that connect these different weather episodes.
37 Here we test this idea. We find that there is indeed a connection between unusually cold weather
38 in Eastern North America and unusually stormy weather and heavy rainfall in Western Continental
39 Europe. We also find a link, albeit weaker, when focussing specifically on extreme events – namely
40 only the coldest of the cold spells, the windiest of the stormy days and the wettest of the heavy
41 rainfall days. The strongest connection, however, emerges when looking at unusual but not
42 extreme weather episodes.

43
44
45
46
47
48
49
50
51

52 **1 Introduction**

53 During recent winters, ostensibly frequent cold spells in Eastern North America (ENA) and wet or
54 windy extremes in Western Continental Europe (WCE) have garnered widespread scientific
55 attention (e.g. Palmer 2014; Lee *et al.*, 2015; Matthias and Kretschmer, 2020; van Oldenborgh *et*
56 *al.*, 2015; Hillier and Dixon, 2020; Owen *et al.*, 2021). These extremes have typically been
57 discussed separately. However, their repeated co-occurrence suggests that they may be spatially
58 compounding extremes, namely geographically remote extremes associated with common
59 physical drivers. Specifically, Messori *et al.* (2016) argued for a link mediated by large-scale
60 atmospheric circulation anomalies over the North Atlantic. However, extreme wet or windy
61 weather in Europe was not explicitly investigated. Later, De Luca *et al.* (2020) focussed on co-
62 occurring cold extremes in ENA and wet extremes in Europe, providing partial support for Messori
63 *et al.* (2016). The study used an approach similar to the one we will adopt here, yet did not consider
64 variables associated with the large-scale atmospheric circulation nor wind extremes. Most recently,
65 Leeding *et al.* (2022) confirmed the repeated co-occurrence of cold spells in North America and
66 wet or windy extremes in Europe, which we hereafter collectively term compound cold–wet–
67 windy extremes, yet again highlighted the need for further analysis of the associated circulation
68 patterns. The current understanding of these compound cold–wet–windy extremes is thus
69 incomplete. Filling this knowledge gap is all the more urgent in view of the growing awareness of
70 the relevance of compound extremes, whose impacts often exceed the sum of those due to the
71 individual events comprising them (Lunt *et al.*, 2016; Zscheischler *et al.*, 2018).

72 The multivariate perspective inherent to compound extremes, adds complexity to conventional
73 statistical tools for the study of extremes (Naveau, 2005). A wide range of approaches have been
74 proposed to deal with multivariate extreme value statistics in climate data, from copula-based
75 methods to max-stable models, conditional exceedance models, machine learning algorithms and
76 more (e.g. Oesting and Stein, 2018; Brunner *et al.*, 2019; Tavakol *et al.*, 2020; Towler *et al.*, 2020;
77 Vogel *et al.*, 2021). Spatially compounding extremes, such as the ones we consider here, present
78 the additional challenge of how to incorporate spatial information into the analysis. Some of the

79 above multivariate statistical approaches may be extended to incorporate spatial information, but
80 this often results in highly complex models (e.g. Genton, 2015; Liu *et al.*, 2021).

81 Here, we leverage dynamical systems theory to provide an analytically and computationally
82 efficient, spatially resolved analysis of compound cold–wet–windy extremes in ENA and WCE.
83 The approach builds upon recent advances in dynamical systems theory (Faranda *et al.*, 2020a),
84 and allows to compute the instantaneous coupling between different atmospheric variables, which
85 we term *co-recurrence ratio*, or α . In this study, we extend this approach for the first time beyond
86 the bivariate case. We propose this as an effective complement to existing analyses of spatially
87 compounding extremes, which may support our understanding of the interplay between different
88 climate extremes and their physical drivers.

89 We specifically seek to answer the following questions:

90 (i) Do cold spells over ENA and wet or windy extremes over WCE individually emerge as events
91 with a particularly strong coupling to large-scale circulation patterns?

92 (ii) Is there evidence for recurrent large-scale circulation patterns systematically associated with
93 the co-occurrence of these extremes?

94 Concerning the first question, there is a vast literature dealing with large-scale circulation patterns
95 favouring the extremes analysed here (e.g. Haylock and Goodess, 2004; Cellitti *et al.*, 2006; Donat
96 *et al.*, 2010; Grotjahn *et al.*, 2015; Harnik *et al.*, 2016; Smith and Sheridan, 2018; Laurila *et al.*,
97 2021). However, the question of whether the coupling of these extremes with the large-scale
98 circulation is unusually strong relative to other days has not been addressed (with the exception of
99 an exploratory analysis for North America in Faranda *et al.*, 2020a). Concerning the second
100 question, both Messori *et al.* (2016) and Leeding *et al.* (2022) conditioned their large-scale
101 atmospheric analysis only on cold spells in ENA, without explicitly accounting for the circulation
102 associated with the European extremes. We begin by analysing separately North America and

103 Europe, and then explicitly address the spatially compounding nature of the cold–wet–windy
104 extremes.

105 **2 Data**

106 We use ECMWF’s ERA5 reanalysis data, over December–January–February (DJF) 1979–2020
107 and with a horizontal resolution of 0.5° (Hersbach *et al.*, 2020). We consider 2-metre temperature
108 (t2m), 10-metre wind (10m wind), total precipitation (tp) and sea-level pressure (SLP). We chose
109 SLP over geopotential height, as the latter displays long-term trends that could affect the dynamical
110 systems analysis (Faranda *et al.*, 2020b). We compute daily averages from hourly data for surface
111 variables and 6-hourly data for pressure-level variables. Anomalies are defined relative to a daily
112 climatology smoothed using a 15-day running mean (similar to Harnik *et al.*, 2016). The 95th (5th
113 for t2m) percentile of the local anomaly distributions is shown in Fig. S1.

114 The t2m in North America is analysed over $30\text{--}45^\circ\text{N}$ $260\text{--}290^\circ\text{E}$ (grey box in Fig. 1a), while 10-
115 m wind and precipitation in Europe are analysed over $45\text{--}60^\circ\text{N}$ $350\text{--}20^\circ\text{E}$ (grey box in Fig. 2a).
116 These domains approximately follow those used in Messori *et al.* (2016) for ENA cold spells and
117 in Hanley and Caballero (2012) for WCE windstorms, respectively. The same domains are also
118 used for analysing SLP co-recurrences (see Sect. 3). A sensitivity analysis using larger domains is
119 presented in the Supplementary Material. Extreme events in t2m, 10m wind and tp are ranked
120 according to the coldest, wettest or windiest anomalies, either at single gridboxes or averaged over
121 the above analysis domains. Compound extremes are identified as described in Text S3. Unless
122 otherwise specified, we analyse the 50 most extreme events. To avoid counting the same extreme
123 multiple times, we impose a minimum separation of 5 days between successive events, following
124 Messori *et al.* (2022). A similar minimum separation is imposed when selecting high α days..

125 Unless otherwise specified, we test statistical significance of composites by verifying whether at
126 least $2/3$ of composite members have the same sign. Assuming a binomial formula with equal
127 chances for positive and negative anomalies, the probability of obtaining a greater than $2/3$ sign
128 agreement randomly is well below 5%.

129

130 **3 Diagnosing the Coupling of Atmospheric Variables**

131 Our analysis rests on computing the instantaneous coupling of multiple atmospheric variables,
132 termed *co-recurrence ratio*, or α (Faranda *et al.*, 2020a; see also applications in De Luca *et al.*,
133 2020a,b and Messori and Faranda, 2021). Given two variables drawn from a chaotic dynamical
134 system, α measures the extent to which recurrences in one variable correspond to recurrences in
135 the other. For example, α computed for SLP and t2m over a given geographical domain diagnoses
136 how often, given the recurrence of a specific t2m spatial pattern in the domain, one also observes
137 the recurrence of the associated SLP spatial pattern. In other words, if α at a given timestep t in
138 our dataset is large, then every time a t2m pattern similar to the t2m pattern of time t appears in
139 the dataset (a *recurrence*), the SLP pattern at that other time will also resemble the SLP pattern of
140 time t . This may then be interpreted as a high coupling. The converse holds for low α . The co-
141 recurrence ratio may also be computed for more than two variables, and diagnoses the extent to
142 which one observes simultaneous recurrences of all the variables being considered. When
143 computing α for more than two variables, one is thus imposing additional constraints relative to
144 the bivariate case. We therefore expect a trivariate α to display lower values than its bivariate
145 counterpart.

146 Unlike other statistical coupling measures, α is instantaneous in time (local in phase space).
147 Namely, a value of α is obtained for each timestep in the dataset being analysed. When computing
148 α , the number of recurrences is always fixed to be the same for all variables; this makes α
149 independent of the ordering of the variables, and it may thus not be interpreted in terms of
150 causality. The range of the co-recurrence ratio is $0 \leq \alpha \leq 1$. We provide the details of the calculation
151 of α for climate data in Text S1. All α values shown in the figures are anomalies, computed as
152 described in Sect. 2. Distributions of these anomalies are shown in Fig. S2.

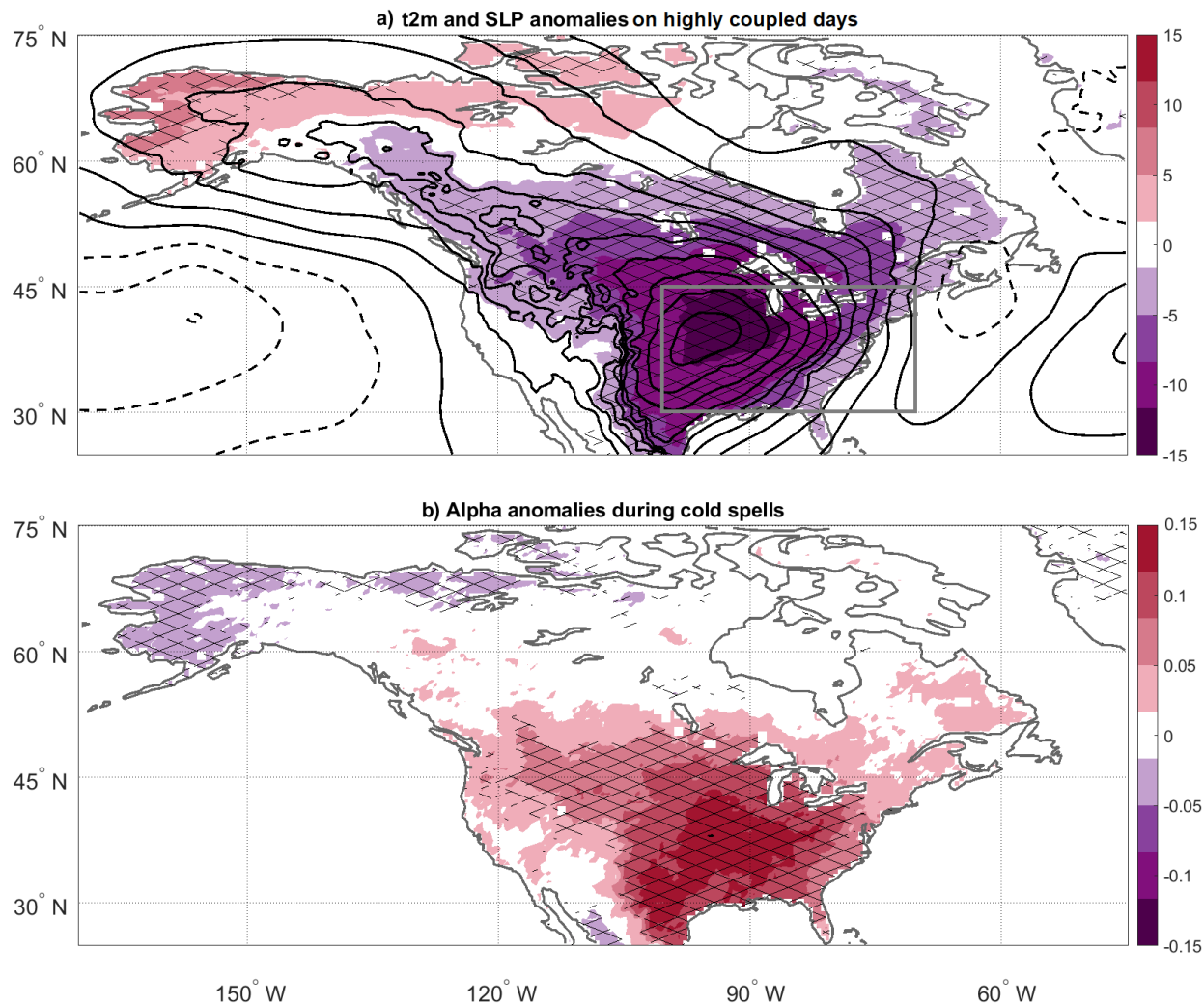
153

154 **4 Large-scale drivers of cold spells in ENA and wet or windy extremes in WCE**

155 **4.1 Individual Extreme Event Classes**

156 We first study separately cold spells in ENA and wet or windy extremes in WCE. To verify how
157 these extremes couple to large-scale atmospheric patterns, we compute α between the relevant
158 impact variable and SLP (Sect. 2). We begin by analysing days on which t2m in ENA is highly
159 coupled to SLP. The 50 days with the highest coupling display an anomalous high pressure centred
160 to the south-west of the Great Lakes region, flanked by two negative pressure anomaly cores (Fig.

161 1a; *cf.* Faranda *et al.*, 2020a). This tripole favours oceanic air mass advection and warm anomalies
162 over Alaska, and simultaneous northerly advection of cold high-latitude air over central-eastern
163 North America. Anomalies in excess of -10 K are attained over ENA, even though we are
164 conditioning solely on α . The large-scale pattern is remarkably similar to that obtained by
165 conditioning on the 50 coldest spells in ENA (Fig. S3a, Tab. S1), and resembles the spatial patterns
166 found by previous studies investigating North American cold spells (*e.g.* Cellitti *et al.*, 2006;
167 Messori *et al.*, 2016; Harnik *et al.*, 2016; Smith and Sheridan, 2018). Additionally, the 50 days
168 with the highest coupling between SLP and t2m show an anomalously frequent occurrence of cold
169 spells over a broad swath of North America (Fig. S4a), and a close overlap with the 50 coldest
170 spells defined at each individual gridbox (not shown). Finally, we compute the $\alpha_{t2m,SLP}$ anomalies
171 associated with the 50 coldest spells at each gridbox (Fig. 1b). The region that shows negative
172 temperature anomalies in Figs. 1a, S3a also displays positive $\alpha_{t2m,SLP}$ anomalies in Fig. 1b. Thus,
173 α shows that the cold spells share a similar spatial footprint and are systematically associated with
174 a recurrent SLP configuration. We conclude that the occurrence of cold spells in ENA is
175 systematically associated with a stronger than usual coupling between SLP and t2m. The
176 qualitative results are not dependent on the choice of computing $\alpha_{t2m,SLP}$ by using the same
177 geographical domain for both variables. Indeed, if we compute $\alpha_{t2m,SLP}$ using t2m over the cold
178 spell box and the SLP pattern over a much larger North American domain, the results are
179 qualitatively comparable (Fig. S5).

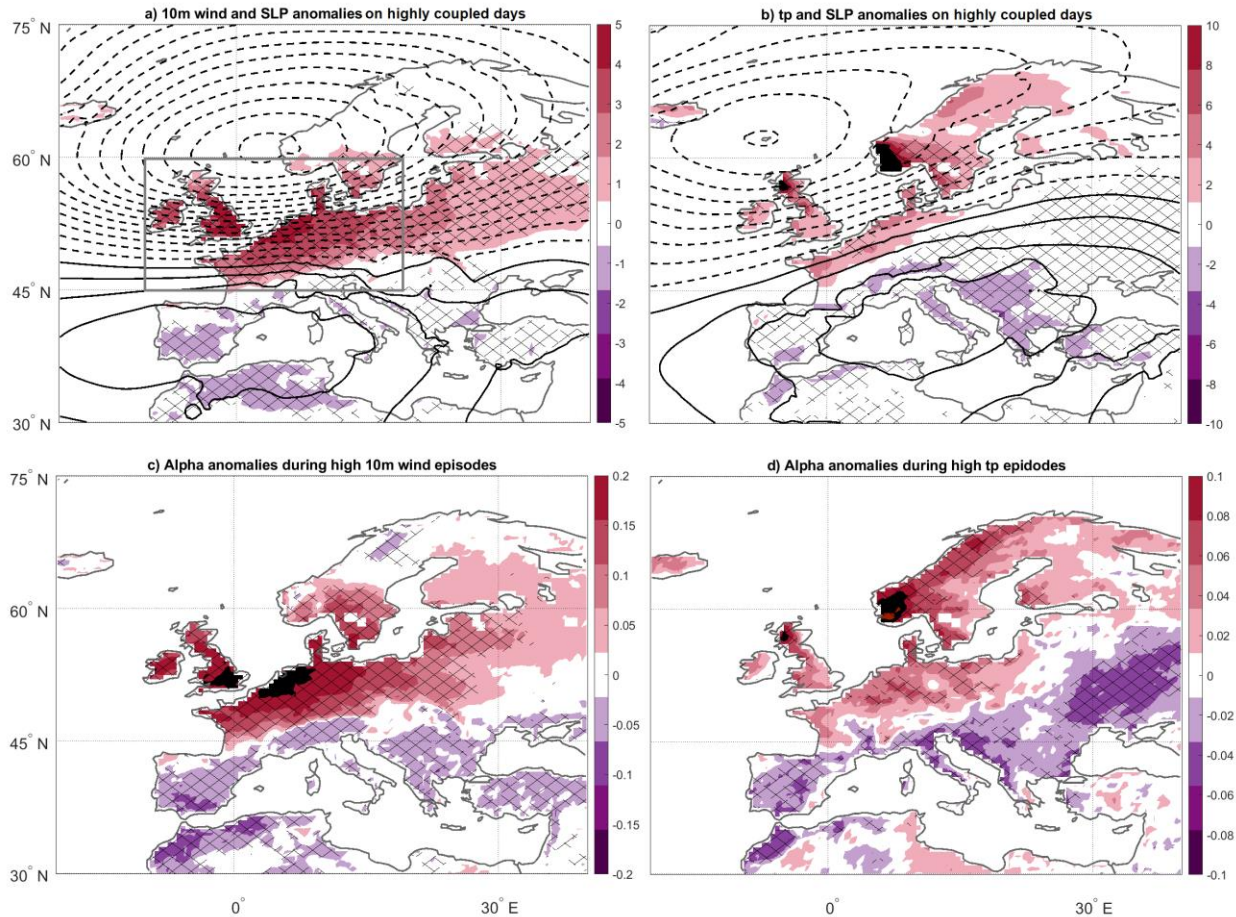


180
 181 **Figure 1.** High t2m–SLP coupling days and cold spell days in ENA. Composite (a) t2m (K,
 182 colours) and SLP (hPa, contours) anomalies for the 50 days displaying the highest $\alpha_{t2m,SLP}$. (b)
 183 Composite $\alpha_{t2m,SLP}$ anomalies for the 50 coldest spells at each gridbox. SLP contours in (a) are
 184 every 2 hPa (negative dashed). Cross-hatching marks regions where at least two thirds of the (a)
 185 t2m and (b) $\alpha_{t2m,SLP}$ anomalies share the same sign. All α are computed over 30–45 °N, 260–290 °E
 186 (grey box in (a)).

187
 188 We next shift the focus to 10m wind and tp anomalies in Europe. The 50 days with the highest
 189 coupling between 10m wind and SLP display strong positive 10m wind anomalies over WCE and
 190 an SLP anomaly dipole with a strong negative core to the south-east of Iceland and a weaker
 191 positive core over the western Mediterranean (Fig. 2a). This eastward-shifted, NAO-like dipole is
 192 typically associated with a zonalised and intensified jet stream, which in turn results in heightened
 193 cyclone frequency and wind destructiveness over Western Europe (Donat *et al.*, 2010; Hanley and
 194 Caballero, 2012; Gómará *et al.*, 2014; Messori and Caballero 2015; Messori *et al.*, 2019). A similar

195 SLP anomaly pattern, albeit with a northward-eastward shifted positive SLP core, is found for the
196 50 days with the highest coupling between tp and SLP (Fig. 2b). Because of the shift in the SLP
197 core, the positive tp anomalies are also shifted slightly northwards relative to the 10m wind
198 anomalies. We reconduct the geographical overlap between the 10m wind and tp anomalies to the
199 dominant role of North Atlantic extratropical cyclones in bringing both strong winds and heavy
200 precipitation to Western Europe, which in turn results in a close relationship between these two
201 classes of extremes (Owen *et al.*, 2021). Indeed, De Luca *et al.*, 2020a explicitly showed that
202 concurrent precipitation–wind extremes match high coupling days computed on precipitation and
203 10m wind over a large part of Western Europe. This relationship emerges here in the form of a
204 high coupling between SLP patterns favouring the presence of cyclones over the continent (see
205 references above) and large 10m wind and tp anomalies there. These SLP, tp and 10m wind
206 anomaly patterns are additionally very similar to those conditioned on the occurrence of tp or 10m
207 wind extremes in WCE (Fig. S3b, c, Tab. S1).

208 We moreover find that the 50 highest coupling days between SLP and the two impact variables
209 correspond to an anomalously high occurrence of 10m wind and tp extremes over regions similar
210 to those highlighted in Fig. 2a, b (Fig. S4b, c) and show a close overlap with the 50 most extreme
211 10m wind and tp events at each gridbox (not shown). The regions that show strong positive 10m
212 wind and precipitation anomalies in Fig. 2a,b also display positive $\alpha_{10m\ wind, SLP}$ and $\alpha_{tp, SLP}$ anomalies
213 during extremes in the former variables (Fig. 2c, d). In analogy with the cold spells analysis, we
214 interpret this as meaning that the surface wind or precipitation extremes in WCE share common
215 spatial footprints and are systematically associated with recurrent SLP configurations. These
216 configurations are similar for the two classes of extremes. We conclude that the occurrence of wet
217 or windy extremes in WCE is associated with a stronger than usual coupling between SLP and the
218 relevant impact variable. Again, using a larger SLP domain for computing $\alpha_{10m\ wind, SLP}$ and $\alpha_{tp, SLP}$
219 provides qualitatively comparable results (Fig. S6).



220

221 **Figure 2.** Days with high 10m wind or tp coupling with SLP and days with extreme 10m wind and
 222 tp in WCE. Composite (a) 10m wind (m s^{-1} , colours) and SLP (hPa, contours) anomalies for the 50
 223 days displaying the highest $\alpha_{10m\ wind, SLP}$ over WCE. (b) Same as (a) but for tp (mm day^{-1}) during
 224 the 50 days displaying the highest $\alpha_{tp, SLP}$. Composite (c) $\alpha_{10m\ wind, SLP}$ anomalies for the 50 most
 225 extreme 10m wind events at each gridbox. (d) Same as (c) but for $\alpha_{tp, SLP}$ and tp. SLP contours in
 226 (a, b) are every 2 hPa (negative dashed). Cross-hatching marks regions where at least two thirds
 227 of the anomalies shown in colours share the same sign. In Panel (b), days with no precipitation are
 228 not included in the latter calculation. The colour ranges in c, d differ; black shaded regions are
 229 beyond the colourbar limits. All α are computed over 45–60 °N, 35–20 °E (grey box in (a)).
 230

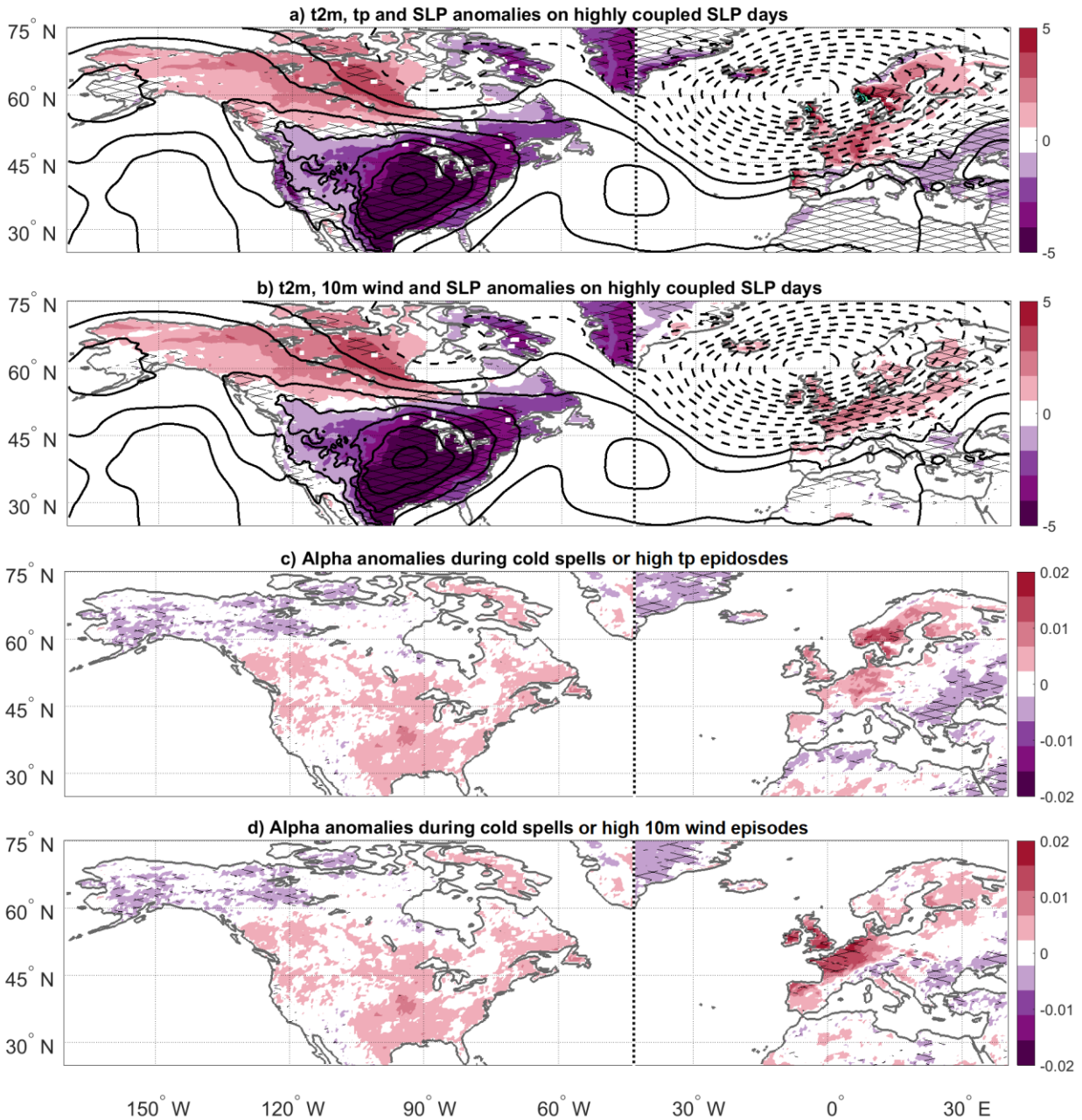
231 4.2 Compound Cold–Wet–Windy Extremes

232 We next consider the link between the cold spells over ENA and the wet or windy extremes over
 233 WCE. In Sect. 4.1, we showed that the individual extreme classes display a close coupling of the
 234 relevant impact variable with the atmospheric circulation as diagnosed by SLP. If the North
 235 American and European extremes are indeed linked through a common large-scale circulation
 236 anomaly pattern, we would expect that both ENA cold spells and WCE wet or windy extremes

237 should match high coupling events between the SLP patterns in the two continents. We thus
238 compute α between North American and European SLP fields. For the 50 highest coupling days,
239 both the SLP anomalies and the t2m, 10m wind and tp anomalies qualitatively match those
240 discussed in Sect. 4.1 (*cf.* Fig. 3a, b with Figs. 1a and 2a, b). The most notable difference is the
241 absence in Fig. 3a, b of weak negative SLP anomalies flanking the North American cold spells.
242 However, the key SLP structures such as the anomalous high over central-eastern North America
243 and the dipole over Europe are very closely reproduced. Similarly, the t2m, 10m wind and tp
244 anomalies only show minor qualitative differences (*e.g.* in central-northern Canada), although they
245 are systematically weaker in magnitude. The same qualitative picture holds if continental-scale
246 domains are used to compute α between North American and European SLPs. However, the
247 additional information given by the simultaneous enlargement of both the North American and
248 European domains leads to the inclusion of SLP structures with little effect on the surface events
249 of interests, and further dilutes the magnitude of the signal (Fig. S7a, b).

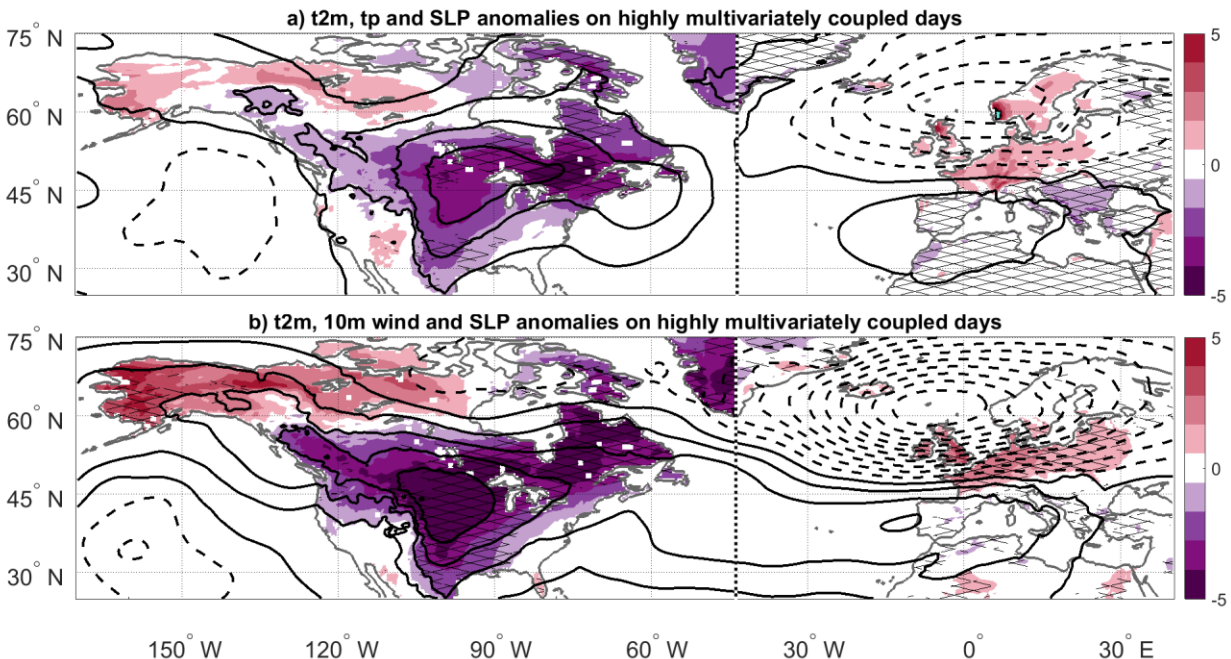
250 The high SLP coupling days between North America and Europe thus show a clear footprint in the
251 surface anomalies. Moreover, the large-scale SLP patterns in Fig. 3a, b are comparable to those
252 conditioned on the occurrence of the top 50 compound cold–wet–windy extremes (Text S3, Fig.
253 S8). However, the link between the high SLP coupling days and the local extreme occurrences is
254 weaker than what observed for the monivariate extremes. This is visible both when computing the
255 occurrence of cold spells, 10m wind or tp extremes during the 50 highest SLP coupling days (*cf.*
256 Figs. S4, S9) and when looking at composite coupling anomalies during the 50 coldest spells or
257 most extreme tp or 10m wind events (*cf.* Figs. 1b, 2c, d and Fig. 3c, d). Specifically, the α anomalies
258 shown in Fig. 3c, d show limited sign agreement, pointing to a large case-by-case variability. The
259 link between the high SLP coupling days and compound cold–wet–windy extremes is generally
260 stronger in WCE than in ENA, with the latter again showing limited sign agreement (Table S2).

261



262
 263 **Figure 3.** Days with high SLP coupling between North America and Europe and days with surface
 264 extremes. Composite (a) t2m (K, colours), tp (mm day⁻¹, colours) and SLP (hPa, contours)
 265 anomalies for the 50 days displaying the highest $\alpha_{SLP1,SLP2}$, where SLP1 is over 30–45 °N, 260–
 266 290 °E and SLP2 is over 45–60 °N, 350–20 °E. The t2m and tp are shown in the left and right-
 267 hand sides of the panel (separated by the vertical dotted line), respectively. (b) Same as (a) but for
 268 10-metre wind (10m wind, m s⁻¹, colours) in the right-hand side of the panel. SLP contours in (a,
 269 b) are every 2 hPa (negative dashed). (c) Composite $\alpha_{SLP1,SLP2}$ anomalies for the 50 coldest spells
 270 or most extreme 10m wind events at each gridbox in the left and right-hand sides of the panel,
 271 respectively. (d) Same as (c) but for tp in the right-hand side of the panel. Cross-hatching marks
 272 regions where at least two thirds of the anomalies shown in colours share the same sign.
 273

274 There is thus mixed evidence for the existence of co-recurrent pan-Atlantic circulation patterns
 275 coupled to the cold spells, 10m wind or tp extremes or the compound cold-wet-windy extremes
 276 analysed here. This may be due to α in Fig. 3 being based only on SLP and not including any of
 277 the impact variables. We thus compute the trivariate co-recurrence for pairs of our impact variables
 278 (t2m and tp and t2m and 10m wind, respectively) and SLP in the respective domains. With the
 279 trivariate coupling, we are requiring a co-recurrence of SLP patterns and surface variable patterns
 280 in two different variables over North American and European domains. The 50 highest trivariate
 281 coupling days display anomalies consistent with those in Fig. 3, albeit somewhat weakened (Fig.
 282 4). The large-scale SLP patterns are comparable to those conditioned on the occurrence of
 283 compound cold-wet-windy extremes (Fig. S8). The link between the high-coupling days and both
 284 classes of compound extremes in WCE again displays high sign agreement, while ENA shows
 285 high sign agreement only for compound cold-wet extremes (Table S2). A sensitivity test on
 286 broader SLP domains over both North America and Europe is shown in Fig. S10. We do not
 287 present here the alpha anomalies associated with extremes in single impact variable as we now
 288 consider more than one impact variable simultaneously in computing the coupling.



289 **Figure 4.** Days with high multivariate coupling between SLP and impact variables in North
 290 America and Europe. As Fig. 3 but for (a) $\alpha_{SLP,t2m,tp}$ and (b) $\alpha_{SLP,t2m,10m\ wind}$, where SLP is taken
 291 jointly over 30–45 °N, 260–290 °E and 45–60 °N, 350–20 °E and the impact variables are taken
 292 over the same domains as in Fig. 3.
 293
 294

295 **5 Discussion and Conclusions**

296 We studied the co-occurrence of cold spells in ENA and wet or windy extremes in WCE by
297 computing the instantaneous coupling between multiple variables, termed *co-recurrence ratio*. It
298 has previously been hypothesised that these extremes are statistically and physically linked
299 (Messori *et al.*, 2016; De Luca *et al.*, 2020a; Leeding *et al.*, 2022). In our analysis, we presented
300 the first implementation of the co-recurrence ratio in a trivariate setting. We framed the study
301 around two questions, namely: whether the individual extreme event classes of interest emerge as
302 having a particularly strong coupling to large-scale atmospheric patterns; and whether there is
303 evidence for recurrent large-scale circulation patterns linking the co-occurrence of these extremes
304 in North America and Europe.

305 Both cold spells in ENA and wet or windy extremes in WCE show an unusually strong coupling
306 to recurrent large-scale atmospheric patterns. Consistent with past literature, the key large-scale
307 features are an anomalous ridge over central North America and an anomalous NAO-like dipole
308 between the North Sea and the Mediterranean. Concerning the second question, our analysis
309 suggests a nuanced picture. Days when the SLP patterns over ENA and WCE are strongly coupled
310 display spatially coherent cold North American anomalies and wet or windy European anomalies,
311 as well as a large-scale circulation resembling that individually associated with cold extremes in
312 ENA and wet or windy extremes in WCE. Nonetheless, the link between the strongly coupled SLP
313 days and extremes in both the individual impact variables we consider and compound extreme
314 occurrences is moderate. Explicitly including the impact variables in the SLP coupling analysis,
315 by computing a trivariate co-recurrence ratio does not markedly increase the link. The condition
316 of co-recurring SLP patterns in ENA and WCE thus leads to a weaker connection to the surface
317 extremes (or, conversely to a weaker connection between surface extremes and coupling
318 anomalies) than in the analyses considering only one continent. Nonetheless, the days with a high
319 trivariate co-recurrence ratio show an anomalously intense, zonal jet that Messori *et al.* (2016) and
320 Leeding *et al.* (2022) hypothesised is key to connecting surface anomalies across the North
321 Atlantic (Fig. S11). We thus conclude that cold ENA anomalies and wet or windy WCE anomalies
322 are closely associated with common, recurrent large-scale atmospheric patterns grounded in a
323 strong coupling between SLP fields over North America and Europe. The same holds to some
324 extent for individual extreme event classes and for compound cold–wet–windy extremes, albeit
325 with a weaker signal. A possible hypothesis is that synoptic-scale drivers which are only indirectly

326 reflected in the large-scale picture – such as extratropical cyclones in the North Atlantic – may
327 significantly modulate the occurrence of the extreme events.

328 Methodologically, our analysis provides a strong complement to more complex multivariate
329 spatial extreme value statistical models. It is time-resolved, and only requires defining one
330 parameter, namely the percentile defining what a *recurrence* is (see Text S1). In the future, the
331 same approach may be extended to study lagged co-recurrence, which would allow to make
332 causality statements. As all approaches, our analysis also displays some caveats. One is the
333 dependence of the quantitative results on the choice of geographical domain. The co-recurrence
334 ratio uses information from the full geographical domain considered, and larger domains will
335 contain information about atmospheric patterns which have little connection with the extremes of
336 interest. Additionally, the theoretical grounding of the calculation of the co-recurrence ratio may
337 pose some challenges to interpreting the results for those not familiar with dynamical systems
338 theory.

339 To conclude compound cold–wet–windy extremes in North America and Europe are only partly
340 governed by a single set of coherent atmospheric circulation patterns. This motivates further
341 analyses focussing specifically on the statistics and drivers of these compound extremes.

342

343 **Acknowledgments**

344 The authors have no conflicts of interest nor financial conflicts related to this work.

345

346 **Open Research**

347 The ERA5 data used in this study is freely available from the Copernicus Climate Change
348 service at:

349 <https://cds.climate.copernicus.eu/cdsapp#!/dataset/reanalysis-era5-single-levels?tab=form>

350 <https://cds.climate.copernicus.eu/cdsapp#!/dataset/reanalysis-era5-pressure-levels?tab=form>

351

352 **References**

- 353 Brunner, M.I., Furrer, R. and Favre, A.-C. (2019) Modeling the spatial dependence of floods using
354 the Fisher copula. *Hydrology and Earth System Sciences*, 23, 107–124.
355 <https://doi.org/10.5194/hess-23-107-2019>
- 356
- 357 Cellitti, M. P., Walsh, J. E., Rauber, R. M., & Portis, D. H. (2006). Extreme cold air outbreaks
358 over the United States, the polar vortex, and the large-scale circulation. *Journal of Geophysical*
359 *Research: Atmospheres*, 111(D2).
- 360
- 361 De Luca, P., Messori, G., Pons, F. M., & Faranda, D. (2020a). Dynamical systems theory sheds
362 new light on compound climate extremes in Europe and Eastern North America. *Quarterly Journal*
363 *of the Royal Meteorological Society*, 146(729), 1636-1650.
- 364
- 365 De Luca, P., Messori, G., Faranda, D., Ward, P. J., Comou, D. (2020b) Compound warm-dry and
366 cold-wet events over the Mediterranean. *Earth System Dynamics*, doi: 10.5194/esd-11-793-2020
- 367
- 368 Donat, M. G., Leckebusch, G. C., Pinto, J. G., & Ulbrich, U. (2010). Examination of wind storms
369 over Central Europe with respect to circulation weather types and NAO phases. *International*
370 *Journal of Climatology*, 30(9), 1289-1300.
- 371
- 372 Faranda, D., Messori, G., and Vannitsem, S. (2019) Attractor dimension of time-averaged climate
373 observables: insights from a low-order ocean-atmosphere model, *Tellus A*, 71, 1–11.
- 374
- 375 Faranda, D., Messori, G., & Yiou, P. (2020a). Diagnosing concurrent drivers of weather extremes:
376 application to warm and cold days in North America. *Climate Dynamics*, 54(3), 2187-2201.
- 377
- 378 Faranda, D., Vrac, M., Yiou, P., Jézéquel, A., & Thao, S. (2020b). Changes in future synoptic
379 circulation patterns: Consequences for extreme event attribution. *Geophysical Research Letters*,
380 47, e2020GL088002. <https://doi.org/10.1029/2020GL088002>
- 381
- 382 Genton, M. G., Padoan, S. A., & Sang, H. (2015). Multivariate max-stable spatial processes.
383 *Biometrika*, 102(1), 215-230.
- 384
- 385 Gómara, I., Rodríguez-Fonseca, B., Zurita-Gotor, P., & Pinto, J. G. (2014). On the relation
386 between explosive cyclones affecting Europe and the North Atlantic Oscillation. *Geophysical*
387 *Research Letters*, 41(6), 2182-2190.
- 388
- 389 Grotjahn, R., et al. (2015), North American extreme temperature events and related large scale
390 meteorological patterns: A review of statistical methods, dynamics, modeling, and trends, *Clim.*
391 *Dyn.*, 1–34.
- 392
- 393 Hanley, J., & Caballero, R. (2012). The role of large-scale atmospheric flow and Rossby wave
394 breaking in the evolution of extreme windstorms over Europe. *Geophysical Research Letters*,
395 39(21).
- 396

- 397 Harnik, N., Messori, G., Caballero, R., & Feldstein, S. B. (2016). The circumglobal North
398 American wave pattern and its relation to cold events in eastern North America. *Geophysical*
399 *Research Letters*, *43*(20), 11-015.
400
- 401 Haylock, M. R., & Goodess, C. M. (2004). Interannual variability of European extreme winter
402 rainfall and links with mean large-scale circulation. *International Journal of Climatology*, *24*(6),
403 759-776.
404
- 405 Hersbach, H., Bell, B., Berrisford, P., Hirahara, S., Horányi, A., Muñoz-Sabater, J., ... & Thépaut,
406 J. N. (2020). The ERA5 global reanalysis. *Quarterly Journal of the Royal Meteorological Society*,
407 *146*(730), 1999-2049.
408
- 409 Hillier, J. K., & Dixon, R. S. (2020). Seasonal impact-based mapping of compound hazards.
410 *Environmental Research Letters*, *15*(11), 114013.
411
- 412 Lau, W. K., & Kim, K. M. (2012). The 2010 Pakistan flood and Russian heat wave: Teleconnection
413 of hydrometeorological extremes. *Journal of Hydrometeorology*, *13*(1), 392-403.
414
- 415 Laurila, T. K., Gregow, H., Cornér, J., & Sinclair, V. A. (2021). Characteristics of extratropical
416 cyclones and precursors to windstorms in northern Europe. *Weather and Climate Dynamics*, *2*(4),
417 1111-1130.
418
- 419 Lee, M. Y., C. C. Hong, and H. H. Hsu (2015), Compounding effects of warm sea surface
420 temperature and reduced sea ice on the extreme circulation over the extratropical North Pacific
421 and North America during the 2013–2014 boreal winter, *Geophys. Res. Lett.*, *42*, 1612–1618.
422
- 423 Leeding, R., Riboldi, J., Messori, G. (2022) On Pan-Atlantic cold, wet and windy compound
424 extremes, *Wea. Clim. Extr.*, 100524.
425
- 426 Liu, Y. R., Li, Y. P., Yang, X., Huang, G. H., & Li, Y. F. (2021). Development of an integrated
427 multivariate trend-frequency analysis method: Spatial-temporal characteristics of climate extremes
428 under global warming for Central Asia. *Environmental Research*, *195*, 110859.
429
- 430 Loikith, P. C., and A. J. Broccoli (2014), The influence of recurrent modes of climate variability
431 on the occurrence of winter and summer extreme temperatures over North America, *Journal of*
432 *Climate*, *27*(4), 1600–1618.
433
- 434 Lucarini, V., Faranda, D., de Freitas, J. M. M., Holland, M., Kuna, T., Nicol, M., ... & Vaienti, S.
435 (2016). *Extremes and recurrence in dynamical systems*. John Wiley & Sons, London.
436
- 437 Lunt, T., Jones, A. W., Mulhern, W. S., Lezaks, D. P., & Jahn, M. M. (2016). Vulnerabilities to
438 agricultural production shocks: An extreme, plausible scenario for assessment of risk for the
439 insurance sector. *Climate Risk Management*, *13*, 1-9.
440
- 441 Matthias, V., & Kretschmer, M. (2020). The influence of stratospheric wave reflection on North
442 American cold spells. *Monthly Weather Review*, *148*(4), 1675-1690.

- 443
444 Messori, G., & Caballero, R. (2015). On double Rossby wave breaking in the North Atlantic.
445 *Journal of Geophysical Research: Atmospheres*, *120*(21), 11-129.
- 446
447 Messori, G., Caballero, R., & Gaetani, M. (2016). On cold spells in North America and storminess
448 in western Europe. *Geophysical Research Letters*, *43*(12), 6620-6628.
- 449
450 Messori, G., Davini, P., Alvarez-Castro, M. C., Pausata, F. S., Yiou, P., & Caballero, R. (2019).
451 On the low-frequency variability of wintertime Euro-Atlantic planetary wave-breaking. *Climate*
452 *Dynamics*, *52*(3), 2431-2450.
- 453
454 Messori, G. and Faranda, D. (2021). Technical note: Characterising and comparing different
455 palaeoclimates with dynamical systems theory. *Climate of the Past*, *17*, 545–563,
456 <https://doi.org/10.5194/cp-17-545-2021>.
- 457
458 Messori, G., Kretschmer, M., Lee, S. H., and Matthias, V. (2022). Stratospheric Wave Reflection
459 Events Modulate North American Weather Regimes and Cold Spells, *Weather and Climate*
460 *Dynamics Discussion*, <https://doi.org/10.5194/wcd-2022-18>.
- 461
462 Naveau, P., Nogaj, M., Ammann, C., Yiou, P., Cooley, D., & Jomelli, V. (2005). Statistical
463 methods for the analysis of climate extremes. *Comptes Rendus Geoscience*, *337*(10-11), 1013-
464 1022.
- 465
466 Oesting, M. and Stein, A. (2018) Spatial modeling of drought events using max-stable processes.
467 *Stochastic Environmental Research and Risk Assessment*, *32*, 63–81.
- 468
469 Owen, L. E., Catto, J. L., Stephenson, D. B., & Dunstone, N. J. (2021). Compound precipitation
470 and wind extremes over Europe and their relationship to extratropical cyclones. *Weather and*
471 *Climate Extremes*, 100342.
- 472
473 Palmer, T. (2014), Record-breaking winters and global climate change, *Science*, *344*(6186), 803–
474 804.
- 475
476 Smith, E. T., & Sheridan, S. C. (2018). The characteristics of extreme cold events and cold air
477 outbreaks in the eastern United States. *International Journal of Climatology*, *38*, e807-e820.
- 478
479 Tavakol, A., Rahmani, V., & Harrington Jr, J. (2020). Probability of compound climate extremes
480 in a changing climate: A copula-based study of hot, dry, and windy events in the central United
481 States. *Environmental Research Letters*, *15*(10), 104058.
- 482
483 Towler, E., Llewellyn, D., Prein, A., & Gilleland, E. (2020). Extreme-value analysis for the
484 characterization of extremes in water resources: A generalized workflow and case study on New
485 Mexico monsoon precipitation. *Weather and Climate Extremes*, *29*, 100260.
- 486

- 487 van Oldenborgh, G.J., Stephenson, D.B., Sterl, A., Vautard, R., Yiou, P., Drijfhout, S.S., von
488 Storch, H. and van den Dool, H. (2015) Drivers of the 2013/14 winter floods in the UK. *Nature*
489 *Climate Change*, 5, 490–491. <https://doi.org/10.1038/nclimate2612>
490
- 491 Vogel, J., Rivoire, P., Deidda, C., Rahimi, L., Sauter, C. A., Tschumi, E., ... & Zscheischler, J.
492 (2021). Identifying meteorological drivers of extreme impacts: an application to simulated crop
493 yields. *Earth system dynamics*, 12(1), 151-172.
494
- 495 Zscheischler, J., Westra, S., Van Den Hurk, B. J., Seneviratne, S. I., Ward, P. J., Pitman, A., ... &
496 Zhang, X. (2018). Future climate risk from compound events. *Nature Climate Change*, 8(6),
497 469-477.